Available online at www.HighTechJournal.org

HighTech and Innovation Journal

Vol. 2, No. 3, September, 2021

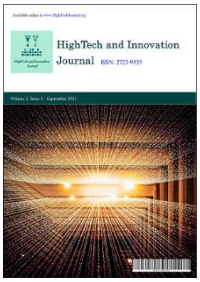

Study of Effect of Size on Iron Nanoparticle by Molecular Dynamics Simulation

Pham Huu Kien [a], Yiachu Khamphone [a], Giap Thi Thuy Trang [a*]

[a] *Department of Physics, Thainguyen University of Education, No. 28 Luong Ngoc Quyen, Thainguyen, Vietnam.*

Received 05 January 2021; Revised 13 April 2020; Accepted 12 May 2021; Published 01 September 2021

Abstract

We use molecular dynamics simulation to study iron Nanoparticles (NPs) consisting of 4000, 5000, and 6000 atoms at temperatures of 300 and 900 K. The crystallization and microstructure were analyzed through the pair radial distribution function (PRDF), the potential energy per atom, the distribution of atom types and dynamical local structure parameters $<f_x>$, where x is the bcc, ico or 14. The simulation indicated that amorphous NP contains a large number of ico-type atoms that play a role in preventing crystallization. Amorphous NP is crystallized through transformations of $f_{14} > 0$ and $f_{bcc} = 0$ type to bcc-type atoms when it is annealed at 900 K upon 40 ns. The growth of crystal clusters happens in parallel with the changing of their microstructure. The behavior of the crystal cluster resembles the nucleation process described by classical nucleation theory. Furthermore, we found that the amorphous NP has two parts: the core has a structure similar to that of amorphous bulk, while the surface structure is more porous and amorphous. Unlike amorphous NP, crystalline NP also has three parts: the core is the bcc, the next part is the distorted bcc and the surface is amorphous. Amorphous and crystalline NPs have part of a core which has a structure that does not depend on size.

Keywords: Nanoparticle; Crystallization; Molecular Dynamics; Amorphous Iron; Effect Size.

1. Introduction

Iron nanoparticle has many attractive properties and finds important applications in different areas of industry. So, the interest in this type of material has continued to grow in recent years [1-3]. NP can be produced in either amorphous or crystalline states. The crystallization process, which plays an important role in modern science and technology [1, 2], has been investigated by both experiment and simulation [4-6]. Computational simulations have been successfully conducted to study the amorphous solid-crystal transitions at atomic levels because simulation has advanced in probing those transitions since it allows calculating the trajectory of individual atoms [7-9].

These studies supplement the commonly used classical nucleation theory (CNT) [10]. For instance, large-scale molecular dynamics (MD) simulations [9] captured the spontaneous nucleation and subsequent grain growth from the atomistic viewpoint. The temperature dependence of nucleation rate and incubation time as obtained from the simulation shows a characteristic shape with nose at critical temperature. The simulation method also has the capability to distinguish structures of different phases using geometric units or cells [11, 12]. Most of these works indicated that CNT can be applied to the crystallization process observed in the simulation, while other works suggested that CNT does not properly describe all aspects of the nucleation process. It was shown that nuclei could be formed through complex pathways and exhibit different structures, shapes, and surface morphology from those assumed in the CNT.

* Corresponding author: tranggtt@tnue.edu.vn

http://dx.doi.org/10.28991/HIJ-2021-02-03-01

In particular, the calculation results of Voronoi polyhedra indicate that the liquid-crystal transition for pure iron comprises the enlargement of the coordination number and a transformation of local symmetry from five-fold to four-fold [13]. In accordance with the simulation [14, 15], the crystallization proceeds by forming a small cluster with a BCC structure, then the core of this cluster transforms into an FCC structure, but the surface has a BCC structure. Other simulations on the binary $Ni_{50}Al_{50}$ system showed that the crystallization proceeds with the formation of initial non-equilibrium long range order regions (LROR) and a subsequent transition to equilibrium LROR [16]. Furthermore, it was revealed that there were multiple intermediate states between disordered and crystalline phases. For the Cu-Ni system [17, 18], the bcc structures act as unstable intermediate states, which are dominated by initial nuclei and eventually transformed into FCC and HCP structures. Such intermediate structures have demonstrated the validity of the step rule of Ostwald.

Although the nanoparticle (NP) has been intensively investigated by simulation and experiment [4-6, 19], the crystallization as well as the microstructure of Fe NP remain poorly understood. Namely, the structure heterogeneity and effect of size on NP are still unclear yet. In the present paper, we develop previous simulations for mechanisms underlying the nucleation and growth of crystals in Fe NP and study the effect of size on iron nanoparticles. The micro-structural evolution is directly traced on the basis of newly proposed dynamical local structure parameters, analyzed in terms of the common neighbor method, transition of different *x-types*, and angle distribution. We also perform a systematic analysis of the temporal structure of crystalline-like clusters in order to identify intermediate states. The local microstructure of amorphous and crystalline NP will also be discussed.

2. Calculation Procedure

We have prepared a NP model at 300 K containing 5000 Fe atoms under free boundary conditions. All atoms are placed in a sphere with a radius of 28 Å. Pak-Doyma potential was used to calculate atomic interactions [20]. We also prepared another model at 900 K. For the convenience of discussion, we call those models as 300- and 900-sample, respectively. The 300-sample was constructed by statistic relaxation and MD simulation [21].

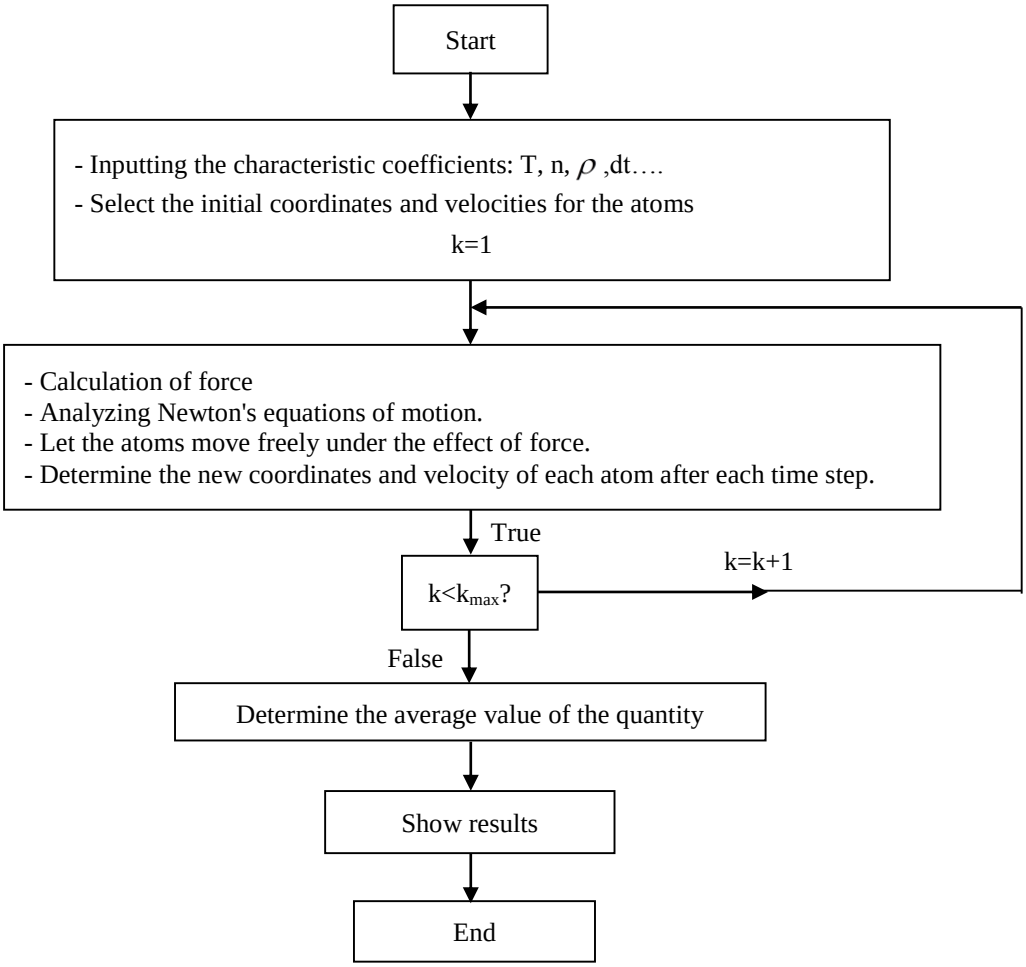

Figure 1. Flowchart of molecular dynamics simulation method

Higher temperature sample is constructed by heating up the 300-sample to desired temperature. Then the obtained sample is isothermally annealed for long time by using NVT ensemble (constant temperature and volume). The annealing time is about 40 ns. The structure characteristics were collected for different configurations during the annealing process. The pair radial distribution function (PRDF) is calculated by the procedure reported in Kodama et al. (2006) [22]. The preparedness for 4000-atoms, 6000-atoms sample at 300, 900K is similar to that for 5000-atoms sample.

We determine the atomic identity (*x*-type) through the coordination cell which consists of a central atom and neighbors. Here the distance between central atom and neighbor is less than cutoff distance r_{cutoff} = 3.35 Å. The cutoff distance is determined from first minimum of PRDF. The atom having 14 neighbor is denoted as 14-type atom. Other *x*-type atoms are identified by CNA method [23].

For instance, the central atom of bcc cell satisfies two conditions: (i) it has 14 neighbors; (ii) six among its neighbors possesses "[4, 4, 4]" and other eight ones have "[6, 6, 6]" numbers where the characteristic numbers indicate respectively the number of common neighbors, number of total bonds between these common neighbors and number of bonds in largest chain of bonds connecting common neighbors. We also determine the *x*-type identity such as bcc-type and ico-type which correspond respectively to the bcc and ico cell. Note that the bcc-type also belongs to 14-type. Due to the atomic rearrangement the identity of every atom can change from one to another x-type during annealing process. To characterize the local environment around particular atom we propose dynamical local structure parameters given as:

$$f_x = \frac{n_x(t_{obs})}{n(t_{obs})} \tag{1}$$

Where $n(t_{obs})$ is the total number of MD steps during the time t_{obs}; $n_x(t_{obs})$ is the number of steps when the identity of given atom is the x-type. For instance, f_{bcc} = 0.9 means that the given atom possesses the bcc-type at about 90% of MD steps within the time t_{obs} [24, 25].

3. Results and Discussion

3.1. Effect of Size for Amorphous Nano

PRDF for 4000-, 5000-, 6000-atoms sample at temperature of 300K is shown in Figure 2. It is clearly that PRDF for samples of different sizes are similar to each other. PRDF fit well the experimental result for amorphous iron: the second peak is split into two sub-peaks. The left sub-peak is higher than the right one. The splitting of second peak may be related to large amount of ico-type atoms which play a role in the preventing of the transformation from amorphous to crystalline phase [8].

For a more detailed understanding of the microstructure of iron amorphous nanoparticle, we consider distribution of atoms, ico-atoms and dynamical local structure parameters $<f_{14}>$, $<f_{ico}>$ for 4000, 5000, 6000 atoms sample through concentric spherical layers in Fig.3 and Fig.4. The characteristic lines of 4000, 5000, 6000 atoms samples are the same with r < 14 Å. So, amorphous NP has part core (r < 14 Å) which has the structure not depend on size and the surface has more porous structure.

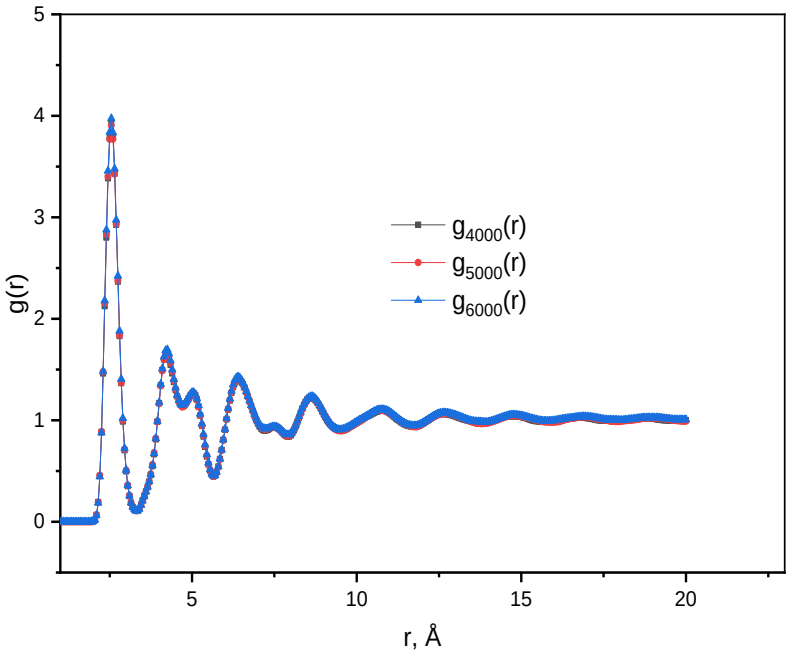

Figure 2. PRDF for 4000, 5000, 6000 atoms sample at 300 K

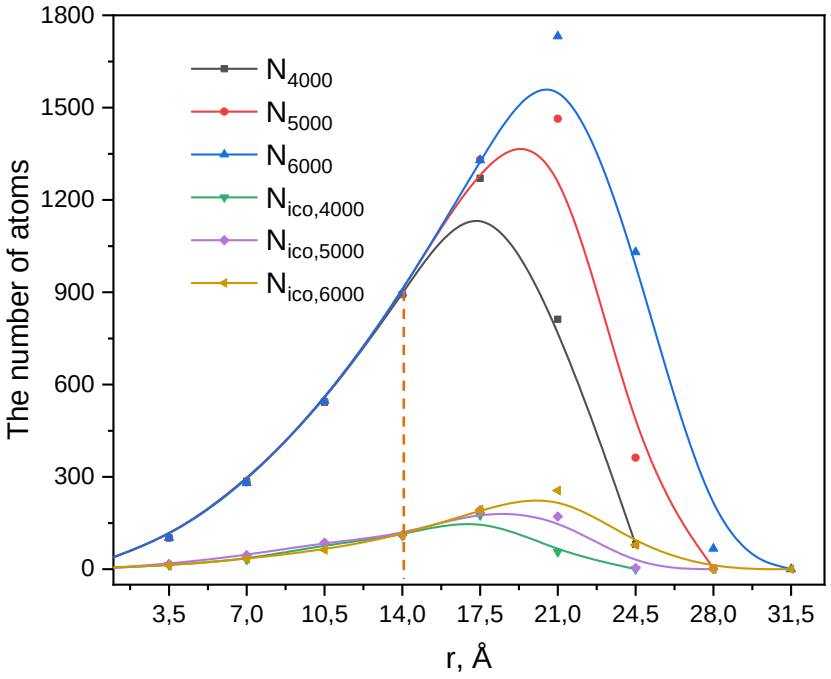

Figure 3. Distribution of atoms, ico-atoms for 4000, 5000, 6000 atoms sample through concentric spherical layers at 300 K

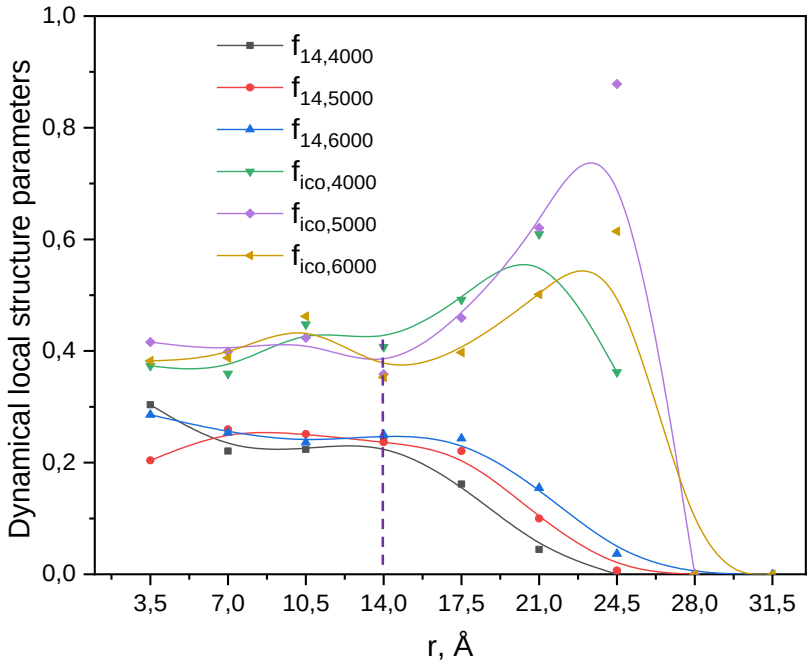

Figure 4. Dynamical local structure parameters <f14>, <fico> for 4000, 5000, 6000 atoms sample through concentric spherical layers at 300 K

3.2. Effect of Size for Crystalline Nan

In Figure 5 we plot the potential energy per atom E_{pot} as a function of annealing time. In the case of 300-sample the curve is nearly straight line and E_{pot} slightly fluctuates around -1.292, -1.300 and -1.305 eV of 4000, 5000 and 6000 atoms sample, respectively. Unlike 300-sample, the 900-sample undergoes various structural transformations under annealing to a stable state. Here this process can be divided into three separate stages as demonstrated in Figure 5. Within the first stage (stage 1), the energy E_{pot} moderately varies with time. This indicates that the system is in metastable state. During stage 2, the energy E_{pot} decreases fast. This clearly demonstrates that unlike first stage, the system is in unstable states and transforms to bcc-crystalline phase. The last stage (stage 3) is characterized by that the energy E_{pot} are slightly fluctuated around fix values. This indicates that the crystallization is completed and the system is in a stable state. E_{pot} after crystallization process of 4000, 5000, 6000 atoms sample are decrease from -1.27÷ -1.29 eV.

The crystallization in NP can be seen from PRDF. As shown in Fig.6, many peaks appear at large distance r as the 4000, 5000, 6000 atoms samples at temperature of 900K is annealed for a long time. Compared to PRDF obtained from the bcc lattice we observe that first ($3^{1/2}a/2$) and third ($2^{1/2}a$) peaks are coincided exactly with that from NP, where a is the lattice constant. However, the first and second peaks are not completely separated. Other peaks also reproduce well those of bcc lattice. It is clearly that PRDF for samples of different size are similar to each other.

To determine the structural evolution we divide all atoms into three groups. G1 group includes atoms with $f_{14} = 0$. The atoms having $f_{14} > 0$ and $f_{bcc} = 0$ belong to G2 group, while the G3 group consists of atoms with $f_{bcc} > 0$. For simplicity these atoms are denoted as G1-, G2- and G3-atom, respectively. Obviously, the crystal cluster consists of G3-atoms.

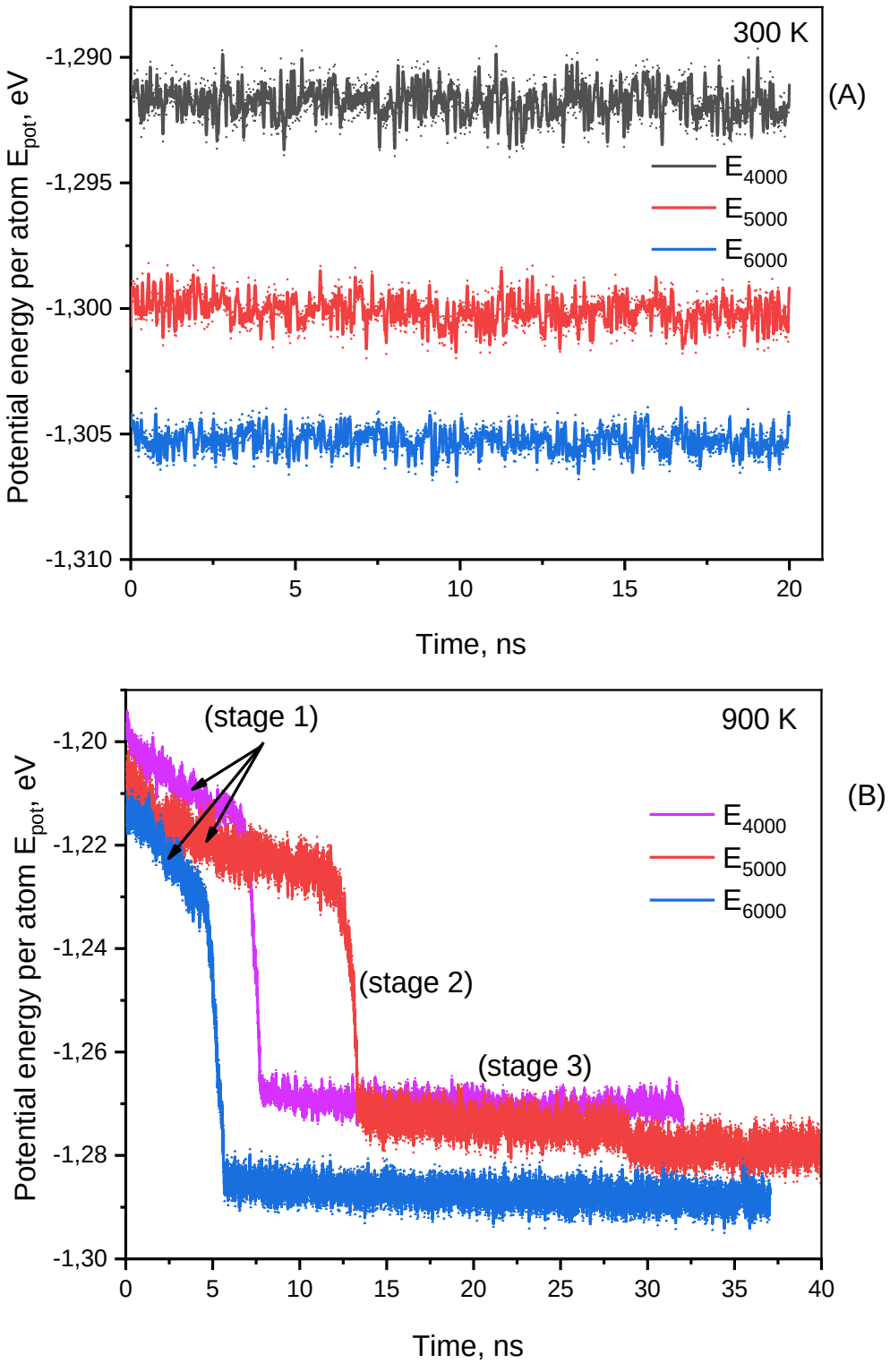

Figure 5. Potential energy per atom as a function of annealing time 4000, 5000, 6000 atoms sample at 300 and 900 K

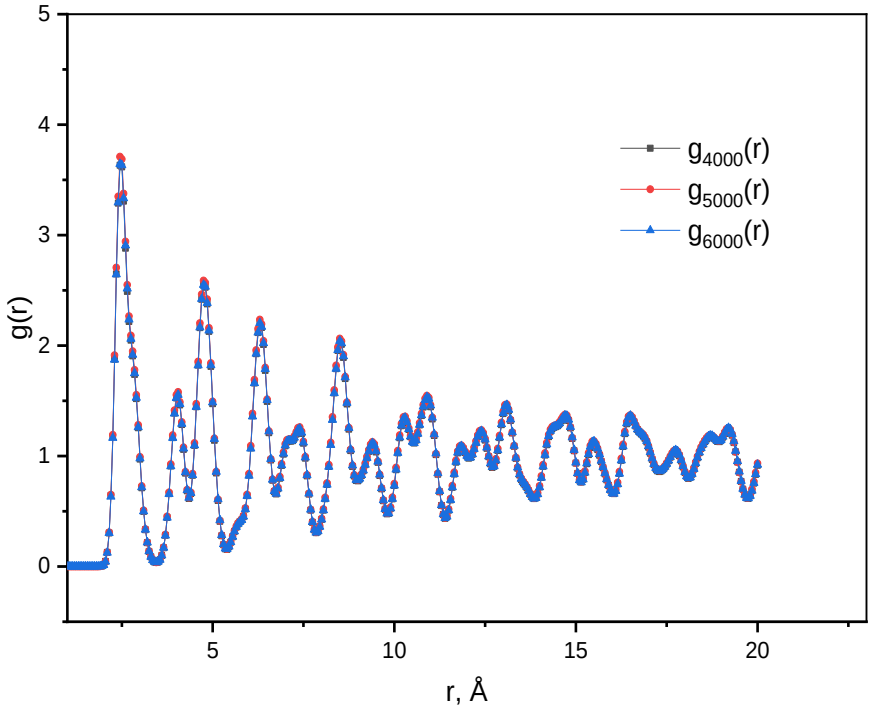

Figure 6. PRDF for 4000, 5000, 6000 atoms sample at 900 K

The characteristics of different type atoms are listed in Table 1. It is crystallized via can be seen that the number of G1-atoms changes slightly with time. In contrast, the G2-atoms convert fast into G3-atoms which mean that NP transformation from amorphous type to bcc-type atoms.

Table 1. Characteristics of atoms of different groups for 5000 atoms sample at 900 K. Here n_{At}, n_{Cl} and s_{LC} is the number of atoms, number of cluster and size of largest cluster, respectively

t, ns	G1			G2			G3		
	n_{At}	n_{Cl}	s_{LC}	n_{At}	n_{Cl}	s_{LC}	n_{At}	n_{Cl}	s_{LC}
2.25	1225	47	1162	3697	1	3697	78	23	29
3.25	1291	52	1220	3591	1	3591	118	19	73
4.25	1334	48	1269	3506	1	3506	160	18	107
5.25	1310	45	1244	3297	2	3296	393	25	351
6.25	1253	30	1215	2921	12	2904	826	15	797
7.25	1246	31	1208	2751	15	2722	1003	15	979
8.25	1218	12	1203	1946	33	1888	1836	17	1802
9.25	1187	4	1184	256	83	24	3557	1	3557
10.25	1250	3	1248	185	91	14	3565	1	3565
11.25	1252	2	1251	191	90	17	3557	1	3557
35.00	1237	1	1237	183	75	15	3580	1	3580

As shown in Table 1, at early time *t*, G3-atoms form a number of clusters, but most among them are small and consist of fewer atoms. There is a large cluster (main cluster) with size significantly larger than other clusters. As the time proceeds, the main cluster grows up, while small clusters either disappear or merge to the main cluster. It is worth to note that unlike amorphous NP, $<f_{ico}>$ for crystalline NP is close to zero. This result confirms the role of ico-atoms for preventing the crystallization.

Table 2 presents the distribution of G3-atoms through concentric spherical layers of NP. It is shown that at early time *t* the main cluster spread is concentrated in layers 14-16, 16-18 and 18-20. Then this cluster grows and is spread over other layers. The main cluster develops from one to other side of NP. At long time *t* the main cluster covers up a major part of NP core.

Table 2. Distribution of G3-atoms through different spherical layers for 5000 atoms sample at 900 K: *a*) all G3-atoms; *b*) the G3-atoms of main cluster

l_{int} - l_{out}	*t* = 2.25 ns		*t* = 5.25 ns		*t* = 7.25 ns		*t* = 8.25 ns	
	a	***b***	***a***	***b***	***a***	***b***	***a***	***b***
0 - 2	0	0	0	0	1	1	2	2
2 - 4	0	0	2	0	9	9	19	19
4 - 6	0	0	4	1	22	22	42	42
6 - 8	0	0	10	8	50	49	73	73
8 - 10	2	0	17	14	66	66	116	116
10 - 12	4	0	37	31	96	93	135	133
12 - 14	13	2	47	41	103	103	177	175
14 - 16	12	4	54	49	130	127	238	230
16 - 18	16	9	63	57	148	144	271	265
18 - 20	19	10	76	72	159	151	342	333
20 - 22	7	2	62	59	157	153	326	319
22 - 24	5	2	20	18	62	61	93	93
24 - 26	0	0	1	1	0	0	2	2

For a more detailed understanding of the microstructure of iron nanoparticle, we consider distribution of atoms, bcc-atoms and dynamical local structure parameters $\langle f_{14} \rangle$, $\langle f_{bcc} \rangle$ for 4000, 5000, 6000 atoms sample through concentric spherical layers as shown in Fig.7 and Fig.8. The characteristic lines of 4000, 5000, 6000 atoms samples are the same with $r < 9$ Å. It can be seen that the size of crystalline NP's core is $r < 9$ Å. It means that, distribution of atoms, bcc-atoms and dynamical local structure parameters in core region don't depend on size of NP.

The amorphous and crystallized NP can be divided into separate regions as schematically described in Figure 9. The amorphous sample consists of surface and core. Unlike the core, the surface has a porous amorphous structure. The crystallized sample comprises three regions. The region located in the surface having the amorphous structure, the next part is distorted and the last region is bcc structure.

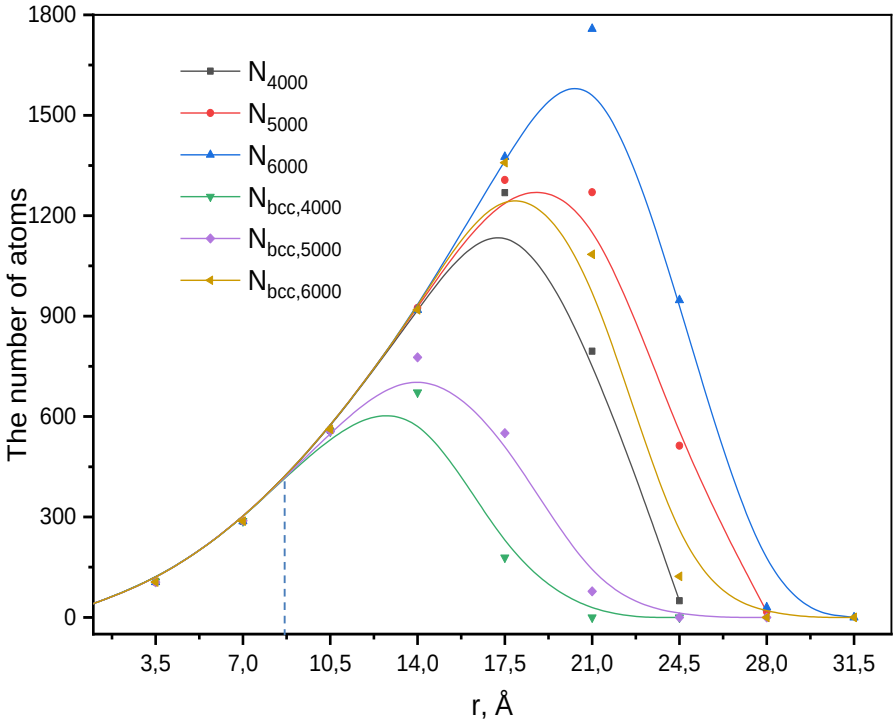

Figure 7. Distribution of atoms, bcc-atoms for 4000, 5000, 6000 atoms sample through concentric spherical at 900 K

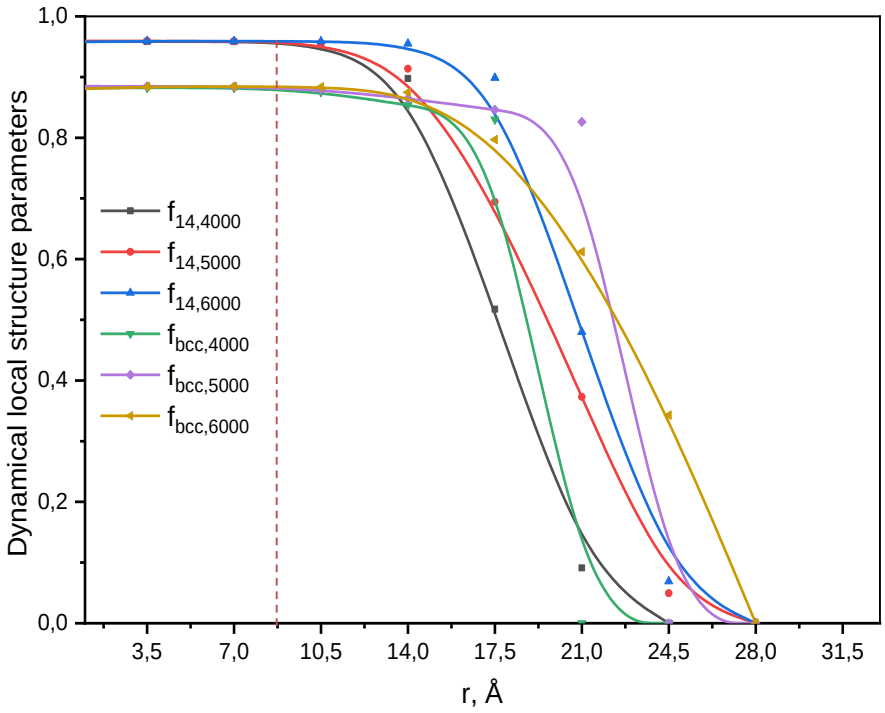

Figure 8. Dynamical local structure parameters <f_{14}>, <f_{bcc}> for 4000, 5000, 6000 atoms sample through concentric spherical at 900 K

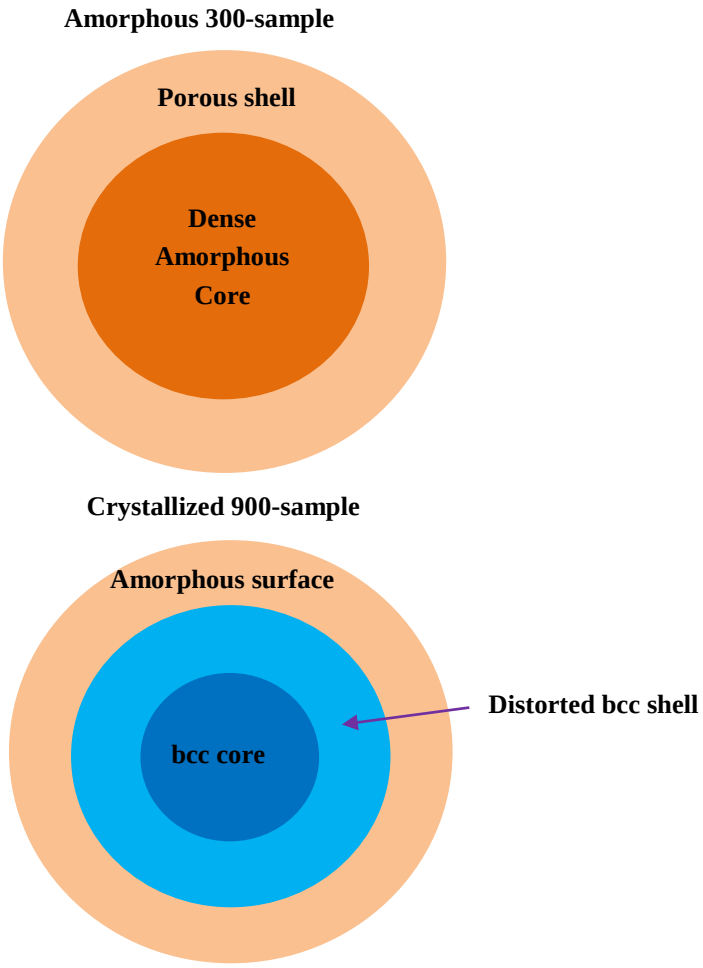

Figure 9. Schematics of separate regions with different microstructure

4. Conclusion

In this study, the annealing of Fe NP consisted of 4000, 5000, 6000 atoms at temperatures of 300 and 900 K has been simulated. When the amorphous NP is annealed at 900 K, it possesses various meta-stable states which differ strongly in the fraction and spatial distribution of low- and high-coordination atoms and the structural transformations that happen. Unlike amorphous NP, $<f_{ico}>$ for crystalline NP is close to zero. This result confirms the role of ico-type atoms in preventing the crystallization and indicates that NP tends to crystallize into a BCC-crystal structure. On the other hand, the specified atoms form a number of clusters, but most of these atoms belong to a large cluster, and small clusters contain only a few atoms. The main cluster spread is concentrated in the middle layers. In the annealing process, this cluster grows and covers up a major part of the NP core, while small clusters either disappear or merge into the main cluster. We have indicated that the structure of the amorphous and crystalline NPs is divided into some separate regions. The first region is located near the surface of NP. The remaining region is called the core, and its size is unchanged by the number of atoms of NP. Besides, we also found that the amorphous NP has two parts: the core has a structure similar to that of amorphous bulk with a smaller radius 14 Å, in while the surface structure is more porous and amorphous. The crystalline NP also has three parts: the core is the bcc with the smaller radius 9 Å, the next part is the distorted BCC, and the surface is amorphous.

5. Declarations

5.1. Data Availability Statement

The data presented in this study are available in article.

5.2. Funding

This work was supported by the Research program of Science and Technology of Thai Nguyen University of Education in 2021 (Grant CS-2021).

5.3. Declaration of Competing Interest

The authors declare that they have no known competing financial interests or personal relationships that could have appeared to influence the work reported in this paper.

6. References

[1] Gharibshahian, E. (2020). The Effect of Polyvinyl Alcohol Concentration on the Growth Kinetics of KTiOPO4 Nanoparticles Synthesized by the Co-precipitation Method. HighTech and Innovation Journal, 1(4), 187–193. doi:10.28991/hij-2020-01-04-06.

[2] Liu, Y., RamaRao, N., Miller, T., Hadjipanayis, G., & Teplyakov, A. V. (2013). Controlling Physical Properties of Iron Nanoparticles during Assembly by “Click Chemistry.” The Journal of Physical Chemistry C, 117(39), 19974–19983. doi:10.1021/jp406021z.

[3] Kien, P. H., Lan, M. T., Dung, N. T., & Hung, P. K. (2014). Annealing study of amorphous bulk and nanoparticle iron using molecular dynamics simulation. International Journal of Modern Physics B, 28(23), 1450155. doi:10.1142/s0217979214501550.

[4] Madras, G., & McCoy, B. J. (2007). Kinetic Model for Transformation from Nanosized Amorphous TiO2to Anatase. Crystal Growth & Design, 7(2), 250–253. doi:10.1021/cg060272z.

[5] Epifani, M., Pellicer, E., Arbiol, J., Sergent, N., Pagnier, T., & Morante, J. R. (2008). Capping Ligand Effects on the Amorphous-to-Crystalline Transition of CdSe Nanoparticles. Langmuir, 24(19), 11182–11188. doi:10.1021/la801859z.

[6] Li, X., & Huang, J. (2003). Molecular dynamics studies of the kinetics of phase changes in clusters III: structures, properties, and crystal nucleation of iron nanoparticle Fe331. Journal of Solid State Chemistry, 176(1), 234–242. doi:10.1016/s0022-4596(03)00414-6.

[7] Delhommelle, J. (2011). Crystal nucleation and growth from supercooled melts. Molecular Simulation, 37(7), 613–620. doi:10.1080/08927022.2011.566611.

[8] Han, J., Wang, C., Liu, X., Wang, Y., Liu, Z.-K., & Jiang, J. (2015). Atomic-Level Mechanisms of Nucleation of Pure Liquid Metals during Rapid Cooling. ChemPhysChem, 16(18), 3916–3927. doi:10.1002/cphc.201500699.

[9] Shibuta, Y., Oguchi, K., Takaki, T., & Ohno, M. (2015). Homogeneous nucleation and microstructure evolution in million-atom molecular dynamics simulation. Scientific Reports, 5(1). doi:10.1038/srep13534.

[10] Kelton, K. F. (2013). Crystal nucleation in supercooled liquid metals. International Journal of Microgravity Science and Application, 30(1), 11-18. doi:10.15011/jasma.30.1.11.

[11] Han, J., Wang, C., Liu, X., Wang, Y., Liu, Z.-K., & Jiang, J. (2015). Atomic-Level Mechanisms of Nucleation of Pure Liquid Metals during Rapid Cooling. ChemPhysChem, 16(18), 3916–3927. doi:10.1002/cphc.201500699.

[12] Tian, Z. A., Liu, R. S., Dong, K. J., & Yu, A. B. (2011). A new method for analyzing the local structures of disordered systems. EPL (Europhysics Letters), 96(3), 36001. doi:10.1209/0295-5075/96/36001.

[13] Pan, S.-P., Feng, S.-D., Qiao, J.-W., Wang, W.-M., & Qin, J.-Y. (2015). Crystallization pathways of liquid-bcc transition for a model iron by fast quenching. Scientific Reports, 5(1), 16956. doi:10.1038/srep16956.

[14] Jungblut, S., & Dellago, C. (2011). Crystallization of a binary Lennard-Jones mixture. The Journal of Chemical Physics, 134(10), 104501. doi:10.1063/1.3556664.

[15] Jabbarzadeh Sani, M. (2021). Spin-Orbit Coupling Effect on the Electrophilicity Index, Chemical Potential, Hardness and Softness of Neutral Gold Clusters: A Relativistic Ab-initio Study. HighTech and Innovation Journal, 2(1), 38–50. doi:10.28991/hij-2021-02-01-05.

[16] An, S., Li, J., Li, Y., Li, S., Wang, Q., & Liu, B. (2016). Two-step crystal growth mechanism during crystallization of an undercooled Ni50Al50 alloy. Scientific Reports, 6(1). doi:10.1038/srep31062.

[17] Zhou, L., Yang, R., Tian, Z., Mo, Y., & Liu, R. (2017). Molecular dynamics simulation on structural evolution during crystallization of rapidly super-cooled Cu50Ni50 alloy. Journal of Alloys and Compounds, 690, 633–639. doi:10.1016/j.jallcom.2016.08.173.

[18] Celik, F. A. (2013). Cooling rate dependence of the icosahedral order of amorphous CuNi alloy: A molecular dynamics simulation. Vacuum, 97, 30–35. doi:10.1016/j.vacuum.2013.04.004.

[19] Shibuta, Y., & Suzuki, T. (2008). A molecular dynamics study of the phase transition in bcc metal nanoparticles. The Journal of Chemical Physics, 129(14), 144102. doi:10.1063/1.2991435.

[20] Hoang, V. V. (2009). Molecular dynamics simulation of liquid and amorphous Fe nanoparticles. Nanotechnology, 20(29), 295703. doi:10.1088/0957-4484/20/29/295703.

[21] Trang, G. T. T., Linh, N. H., Linh, N. T. T., & Kien, P. H. (2020). The Study of Dynamics Heterogeneity in SiO2 Liquid. HighTech and Innovation Journal, 1(1), 1–7. doi:10.28991/hij-2020-01-01-01.

[22] Kodama, K., Iikubo, S., Taguchi, T., & Shamoto, S. (2006). Finite size effects of nanoparticles on the atomic pair distribution functions. Acta Crystallographica Section A Foundations of Crystallography, 62(6), 444–453. doi:10.1107/s0108767306034635.

[23] Stukowski, A. (2012). Structure identification methods for atomistic simulations of crystalline materials. Modelling and Simulation in Materials Science and Engineering, 20(4), 045021. doi:10.1088/0965-0393/20/4/045021.

[24] Trang, G. T. T., Kien, P. H., Hung, P. K., & Ha, N. T. T. (2020). Molecular dynamics simulation of microstructure and atom-level mechanism of crystallization pathway in iron nanoparticle. Journal of Physics: Conference Series, 1506, 012020. doi:10.1088/1742-6596/1506/1/012020.

[25] Giap Thi Thuy Trang, Pham Khac Hung, and Pham Huu Kien (2019). About microstructure and crystallization pathway in iron nanoparticle under temperature. The 6th Academic Conference on Natural Science for Young Scientists, Master and PhD Students from Asean Countries (CASEAN - 6), 23rd-26th Octorber, (2019) at Thai Nguyen University, Thai Nguyen City, Vietnam.